Journal of Materials Chemistry A

RSC Publishing

PAPER

View Article Online
View Journal | View Issue

Cite this: *J. Mater. Chem. A*, 2013, **1**, 282

Controlled synthesis of concave Cu_2O microcrystals enclosed by {*hhl*} high-index facets and enhanced catalytic activity†

Xue Wang, Chang Liu, Binjie Zheng, Yaqi Jiang, Lei Zhang, Zhaoxiong Xie* and Lansun Zheng

Received 9th September 2012
Accepted 27th September 2012

DOI: 10.1039/c2ta00241h

www.rsc.org/MaterialsA

Due to the fact that crystal facets with high surface energy usually exhibit superior performance in many fields, such as catalysis, the importance of the synthesis of micro/nano-crystals with exposed high surface energy facets is becoming a hot research field. In this article, concave Cu_2O microcrystals mainly enclosed by {*hhl*} high-index facets have been successfully prepared by reducing $Cu(CH_3COO)_2$ with glucose in the presence of sodium dodecyl sulphate (SDS). SDS was proved to be important in the formation of the concave Cu_2O microcrystals. The concave degree of truncated octahedra can be controlled by adjusting the concentration of SDS. In addition, we found the reaction rate also affected the morphology of Cu_2O microcrystals. Octahedron-based branched particles, truncated concave octahedra and truncated octahedra can be obtained by adjusting the concentration of glucose. In the catalytic oxidation of CO, truncated concave octahedral Cu_2O enclosed by {332} high-index facets exhibited the highest catalytic activity among the high-index {332} facets, low index {111} and {100} facets, due to the existence of high density steps on {332} facets and the CO catalytic activities of the crystal facets are in the sequence: {332} > {111} > {100}.

Introduction

The surface atomic structure of crystalline materials is one of the important factors that influence their properties. Microcrystals and nanocrystals enclosed by high energy facets usually exhibit high activities, owing to the existence of abundant unsaturated coordination atoms and atomic steps and ledges.[1–3] However, the high energy facets usually diminish during the growth process due to minimization of crystal surface energy. Therefore, how to synthesize microcrystals and nanocrystals enclosed by high energy facets is a challenging research topic, and has attracted more and more attention. In the past few years, great efforts have been made in the syntheses of noble metal and metal oxide microcrystals and nanocrystals exposed with high-index (high surface energy) facets.[4–27] Due to relatively weak metal–metal bonds, the control of noble metal with exposed high-index facets has made great progress recently.[4–18] However, the control of high energy facets of metal oxide microcrystals and nanocrystals is difficult, owing to the strong metal–oxygen bonds. To date, only a few successful examples, such as Co_3O_4, anatase TiO_2, Fe_3O_4, Fe_2O_3, Cu_2O and SnO_2, have been reported,[20–27] and the synthesis of the metal oxides with exposed high energy facets is still a challenge.

Cuprous oxide (Cu_2O), a p-type semiconductor with the bandgap of 2.17 eV, has been widely used in the fields of photocatalysis, water splitting, solar energy conversion, lithium-ion batteries and catalysis.[24,28–34] Due to the propensity of valence variations, Cu_2O can readily seize or release surface lattice oxygen, which may result in the higher CO oxidation catalytic activities compared to Cu and CuO.[35] To date, various Cu_2O microcrystals and nanocrystals, such as cubes, octahedra, rhombic dodecahedra and hexapods have been reported.[28,36–41] However, the obtained Cu_2O microcrystals and nanocrystals are enclosed by low-index facets such as {100}, {111} and {110}. Very recently, Wang and co-workers have reported the synthesis of 50-facet Cu_2O microcrystals partially enclosed by {311} high-index facets, and found that the {311} high-index facets exhibit higher catalytic activities.[24] To further study the relationship

Key Laboratory for Physical Chemistry of Solid Surfaces & Department of Chemistry, College of Chemistry and Chemical Engineering, Xiamen University, Xiamen 361005, China. E-mail: zxxie@xmu.edu.cn; Fax: +86-592-2183047; Tel: +86-592-2180627

† Electronic supplementary information (ESI) available: Schematic model of Cu_2O (332) surface projected along the [$\bar{1}$10] direction, SEM images of truncated concave octahedral Cu_2O microcrystals and cubic Cu_2O microcrystals, high-magnification SEM images and models of the truncated concave octahedral Cu_2O exposed with 24 {332} and six {100} facets viewed from different directions, TEM characterization of truncated concave octahedral Cu_2O microcrystals by using 0.005 M SDS, photographs showing the change in the solution color as a function of reaction time in the synthesis of four types of Cu_2O in Fig. 3, specific oxidation rates of CO over Cu_2O microcrystals with different morphologies at different temperatures, XRD patterns and SEM images of three types Cu_2O microcrystals after catalytic CO oxidation up to 220 °C, and XPS results of Cu2p of Cu_2O microcrystals before and after catalytic CO oxidation. See DOI: 10.1039/c2ta00241h

between surface structures and catalytic activities, the syntheses of Cu_2O enclosed by other high-index facets become more and more important.

In this paper, we developed a facile wet chemical method to synthesize truncated concave octahedral Cu_2O microcrystals mainly enclosed by {*hhl*} high-index facets. The effects of surfactant and reduction rate on the morphology of Cu_2O were studied and discussed. In addition, catalytic activities of Cu_2O with different morphologies were measured and, based on the surface atomic structures, the relationship between the exposed facets of materials and their catalytic performance was discussed.

Experimental

Materials

Copper(II) acetate monohydrate ($Cu(CH_3COO)_2 \cdot H_2O$, 99%) was purchased from Shantou Xilong Chemical Reagent Co., Ltd. Sodium hydroxide (NaOH, 96%) was purchased from Guangdong Guanghua Sci-Tech Co., Ltd. Sodium dodecyl sulphate (SDS, 86%), D-(+)-glucose (analytical grade), copper(II) chloride dihydrate ($CuCl_2 \cdot 2H_2O$, analytical grade) and L-ascorbic acid (analytical grade) were purchased from Sinopharm Chemical Reagent Co., Ltd. All chemicals were used as received without further purification.

Synthesis of truncated concave octahedral Cu_2O microcrystals enclosed by 24 {*hhl*} high-index facets and six {100} facets

In a typical synthesis, deionized water (8.82 mL), $Cu(CH_3COO)_2$ aqueous solution (0.50 mL, 0.10 M), and SDS (0.087 g) were successively added to a sample vial. The sample vial was placed in a water bath set at 60 °C with vigorous stirring. After complete dissolution of SDS powder, NaOH solution (0.18 mL, 1.00 M) and D-(+)-glucose aqueous solution (0.50 mL, 0.10 M) were successively added to the vial. The volume of the final solution was 10 mL and the concentration of the SDS surfactant in the final solution was 0.03 M. Then the vial was stirred for half a minute and the solutions were further kept in the water bath for 1 h. A brick-red color appeared gradually. When the reaction was finished, the precipitate was separated from the solution by centrifugation at 3000 rpm for 3 min, and washed several times with deionized water. Then the sample was dried under vacuum at ambient temperature.

Synthesis of truncated octahedral Cu_2O microcrystals enclosed by eight {111} and six {100} facets

In a typical synthesis, deionized water (7.72 mL), $Cu(CH_3COO)_2$ aqueous solution (0.50 mL, 0.10 M), and SDS (0.087 g) were successively added to a sample vial. The sample vial was placed in a water bath set at 60 °C with vigorous stirring. After complete dissolution of SDS powder, NaOH solution (0.18 mL, 1.00 M) and D-(+)-glucose aqueous solution (1.60 mL, 0.10 M) were successively added to the vial. The volume of the final solution was 10 mL. Then the vial was stirred for half a minute and the solutions were further kept in the water bath for 1 h. When the reaction was finished, the precipitate was separated from the solution by centrifugation at 3000 rpm for 3 min, and washed several times with deionized water. Then the sample was dried under vacuum at ambient temperature.

Synthesis of cubic Cu_2O microcrystals enclosed by {100} facets

Cubic Cu_2O microcrystals were prepared by the method reported.[30] In a typical synthesis, $CuCl_2 \cdot 2H_2O$ (0.171 g) was dissolved into aqueous solution (100 mL). Then NaOH aqueous solution (10.0 mL, 2.0 M) was added dropwise into the above transparent light green solution. After stirring for 0.5 h, ascorbic acid solution (10.0 mL, 0.6 M) was added dropwise into the above solution. A turbid red liquid gradually formed. The mixture was aged for 3 h. All of the procedures were carried out under constant stirring and heated at 55 °C. The resulting precipitate was separated from the solution by centrifugation at 5000 rpm for 3 min and washed several times with deionized water and ethanol. Then the sample was dried under vacuum at ambient temperature.

Structural characterization

The composition and phase of as-prepared products were acquired from the powder X-ray diffraction (XRD) pattern, recorded on a Panalytical X-pert diffractometer with Cu-Kα radiation. The morphology and crystal structure of the as-prepared products were observed by scanning electron microscopy (SEM, S4800) and high-resolution transmission electron microscopy (HRTEM, JEM 2100) with an acceleration voltage of 200 kV. All TEM samples were prepared by depositing a drop of diluted suspension in distilled water on a copper grid coated with carbon film. The surface compositions of Cu_2O samples were determined by a PHI QUANTUM2000 photoelectron spectrometer (XPS) using a monochromatic magnesium X-ray source. The binding energies were calibrated with respect to the signal for adventitious carbon (binding energy of 284.6 eV).

Catalytic measurements

The catalytic activity of Cu_2O catalysts towards CO oxidation was examined in a continuous flow reactor. The reaction gas, 5% CO in nitrogen (99.999%) (10 mL min^{-1}) and air (99.999%) (40 mL min^{-1}), was fed to catalysts (50 mg) that were set in a fixed-bed flow reactor made of glass with an inner diameter of 2.4 mm. Steady-state catalytic activity was measured at each temperature, with the reaction temperature rising from room temperature to 220 °C in steps of 10 °C. The effluent gas was analyzed on-line by an on-stream gas chromatograph (Ramiin GC 2060) equipped with a TDX-01 column.

Results and discussion

Truncated concave octahedral Cu_2O enclosed by {*hhl*} high-index facets was synthesized *via* a facile wet chemical method using copper(II) acetate as a source, SDS surfactant and glucose as a reducing agent in an alkaline solution of NaOH. Scanning electron microscopy (SEM) image shows that the product consists of truncated concave octahedral particles, the size of which is about 1 μm (Fig. 1a and Fig. S1†). The corners of the concave octahedra are truncated, and the edges are also slightly truncated. The truncated corners have {100} facets exposed and the truncated

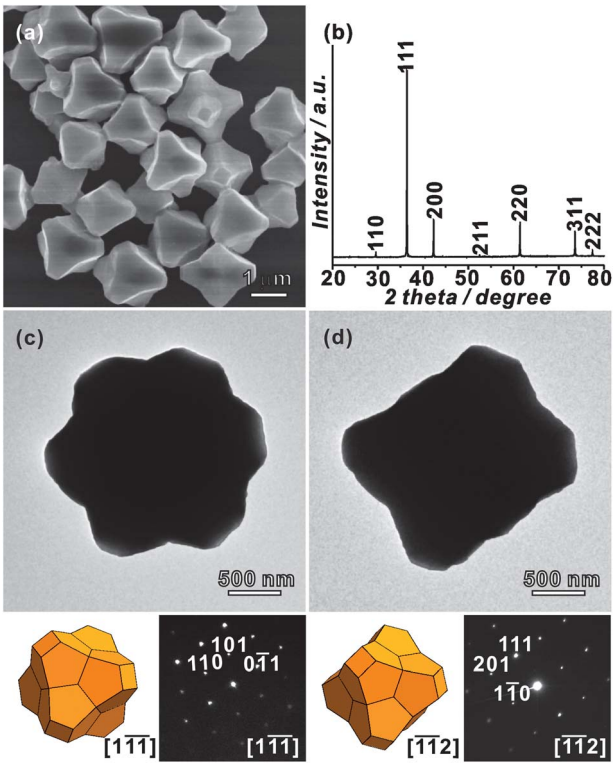

Fig. 1 (a) Typical SEM image and (b) XRD pattern of Cu_2O truncated concave octahedral microcrystals. Typical low-magnification TEM images, corresponding SAED patterns and schematic model of a proposed truncated concave octahedron enclosed by 24 {*hhl*} and six {100} facets viewed along the [1$\bar{1}$$\bar{1}$] direction (c) and [$\bar{1}\bar{1}$2] direction (d).

edges have {110} facets exposed. Due to the fact that the percentage of truncated edges is very small, we neglect the presence of {110} facets in the following discussion. Fig. 1b shows a typical powder X-ray diffraction (XRD) pattern of the as-prepared product, which can be indexed to the cubic phase Cu_2O (JCPDS No. 05-0667). Fig. 1c and d show the typical TEM images and corresponding selected area electron diffraction (SAED) patterns of a truncated concave octahedron, and a proposed truncated concave octahedral model projected along a different zone axis, respectively. The SAED patterns indicate that the as-prepared truncated concave octahedral Cu_2O microcrystals are single crystalline. In the proposed model, the facets in the apex of the concave octahedron are {100} facets and the inclined planes of the concave octahedron are expected to be {*hhl*} ($h > l$) facets. The inclined surfaces are proposed to be {332} facets by matching the schematic model with the observed truncated concave octahedron, where the {332} facet can be described as 2(111) terraces × (110) monoatomic steps by a terrace × step notion (Fig. S2†).[42] The above deduction can be confirmed by matching the proposed model with high-magnification SEM images of some Cu_2O particles in different orientations (Fig. S3†). It can be found that the proposed model matches well outlines of particles in various orientations in the SEM image.

In the proposed synthetic method, an appropriate amount of SDS played an important role in the formation of concave Cu_2O microcrystals. A series of experiments were performed by only changing the concentration of SDS and keeping other conditions unchanged. Without SDS, the obtained Cu_2O microcrystals were not uniform, but most of them were truncated octahedral particles with exposed {111} and {100} low-index facets (Fig. 2a). Meanwhile, some concave cubes formed, and the facets were inclined from the {100} facets. Such concave facets could be described as {*hkk*} ($h > k$) facets, which consist of {100} and {111} terraces and steps. With the addition of SDS, truncated concave octahedral Cu_2O microcrystals enclosed by {*hhl*} ($h > l$) facets appeared. The {*hhl*} facets consist of (111) terraces × (110) steps and thus are structurally different from {*hkk*} facets. When the concentration of SDS was 0.005 M, the as-prepared Cu_2O microcrystals were slightly concave (Fig. 2b) and $h : h : l$ was inclined to 1.08 : 1.08 : 1 (Fig. S4†). With the increase of the concentration of SDS, the concave degree increased. When increasing the concentration of SDS to 0.030 M, truncated concave octahedral particles mainly exposed {332} high-index facets (Fig. 2c). However, the concave degree did not increase when more SDS was added. For example, the morphology of Cu_2O microcrystals did not change if the concentration of SDS was increased to 0.050 M (Fig. 2d).

From the experiment results above, we may conclude that a certain range of concentration of SDS is crucial in the synthesis of Cu_2O with exposed {332} high-index facets in this system. According to the terrace × step notion,[42] the {332} high-index facet can be described as 2(111) terraces × (110) monoatomic steps. SDS might tend to adsorb on the step edge, forming steps consisting of 2(111) terraces × (110) monoatomic steps. Such a step is a basic unit of {332} high-index facets and we denoted it as a (332)-step in the following discussion. In the absence of SDS, no SDS can stabilize the (332)-steps, and thus truncated octahedral particles and concave cubes tend to be formed (Fig. 2a). However, because SDS tended to adsorb {332}-steps, concave octahedra

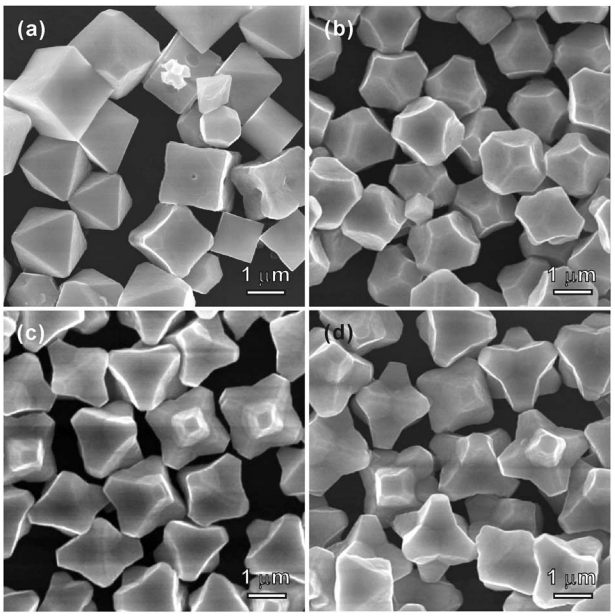

Fig. 2 SEM images of Cu_2O microcrystals synthesized using the conditions for Cu_2O truncated concave octahedra enclosed by 24 {332} and six {100} facets, with different concentrations of SDS: (a) 0; (b) 0.005 M; (c) 0.030 M and (d) 0.050 M.

(consisting of {111} and {110} terraces and steps) instead of concave cubes (consisting of {100} and {111} terraces and steps) appeared when SDS was added. When the concentration of SDS is low, only a few (332)-steps can be formed by the adsorption of SDS, and therefore Cu_2O microcrystals with a small concave degree (Fig. 2b), where the density of (332)-steps is low, are formed. With the increase of concentration of SDS, the density of (332)-steps increases, resulting in the increase of the concave degree. When the concentration of SDS is sufficient (0.030 M), perfect {332} high-index facets with the highest density of (332)-steps are formed. Further increase of the concentration of SDS therefore does not affect the exposed {332} facets any more. From the above experimental results, it can be concluded that SDS plays an important role in the formation of the concave Cu_2O microcrystals resulting from the formation of (332)-steps.

Furthermore, it is found that the concentration of glucose also affects the morphology of Cu_2O microcrystals. As shown in Fig. 3, Cu_2O microcrystals of different morphologies can be obtained by adjusting the concentration of glucose with 0.030 M SDS. When the concentration of glucose was 2 mM, octahedron-based branched Cu_2O particles with a size of about 2 μm were found in the product (Fig. 3a). When the concentration of glucose increased to 5 mM, truncated concave octahedral Cu_2O microcrystals mainly enclosed with {332} high-index facets with the size about 1 μm were obtained (Fig. 3b). Further increase of the concentration of glucose resulted in a decrease of the concave degree (Fig. 3c). When the concentration of glucose increased to 16 mM, the morphology of the obtained Cu_2O microcrystals evolved to truncated octahedra with eight {111} and six {100} low-index facets exposed.

As we know, the reduction and crystal growth rates would increase with the increase of the concentration of glucose. The morphology evolution with the concentration of glucose could be due to the kinetic effects, *i.e.*, the influence of the crystal growth rate. At a very slow growth rate, Cu_2O tends to form branched structures, while isolated polyhedral particles form with the increase of growth rate (Fig. S5–S8†). In addition, the growth rate could also affect the concave degree. In one of our previous studies about the morphology evolution of Cu_2O *via* using an electrochemical reduction method in the absence of any surfactant, we also found the morphology was changed by the deposition current (corresponding to the growth rate).[43] Similar branched particles formed at low reduction currents, while isolated polyhedral particles formed at high reduction currents, which is consistent with the present results if we consider the kinetic effects. However, how the growth kinetics affects the morphology of Cu_2O particles is still unclear.

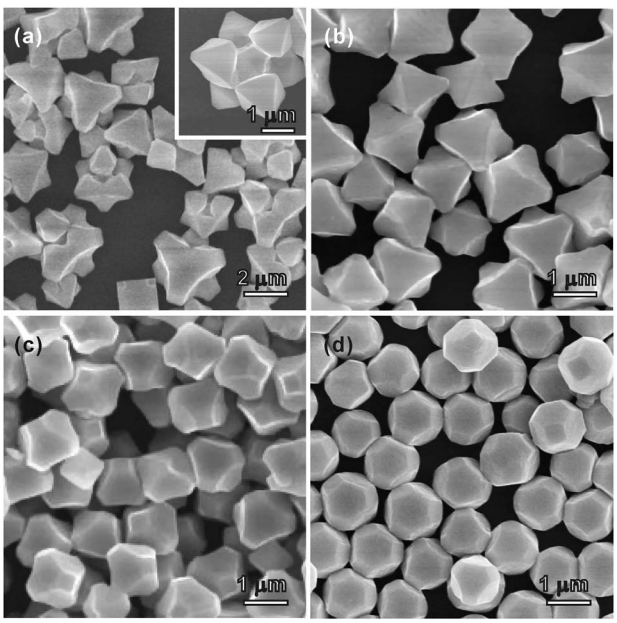

Fig. 3 SEM images of Cu_2O microparticles synthesized using different concentrations of glucose with 0.030 M SDS: (a) 2 mM; (b) 5 mM; (c) 8 mM and (d) 16 mM.

As we know, the catalytic activity depends on the surface structure of the material and different surface structures may result in different catalytic activities. As there are high-density atomic steps on {332} high-index surfaces, truncated concave octahedra enclosed mainly by {332} facets are expected to exhibit high chemical activity. To investigate the surface effect on the catalytic properties of Cu_2O, the catalytic oxidation of CO was chosen as the probe reaction. Truncated concave octahedral Cu_2O enclosed by 24 {332} facets and six {100} facets denoted as truncated concave octahedral Cu_2O {332} + {100}, truncated octahedral Cu_2O exposed with eight {111} facets and six {100} facets denoted as truncated octahedral Cu_2O {111} + {100}, and cubic Cu_2O with exposed {100} facets denoted as cubic Cu_2O {100} (Fig. S9†) were used as catalysts. The catalytic CO oxidation over the three kinds of Cu_2O microcrystals was evaluated in a CO/Air/N_2 stream, the as-prepared Cu_2O microcrystals with the same mass were used in the test. The reaction temperature was raised from room temperature to 220 °C in steps of 10 °C. As shown in Fig. 4a, truncated concave octahedral Cu_2O {332} + {100} exhibited the highest catalytic activity, whereas cubic Cu_2O {100} showed the lowest catalytic activity. Truncated concave octahedral Cu_2O {332} + {100} becomes active at 170 °C and achieves a CO conversion of 50.4% at 220 °C. And truncated octahedral Cu_2O {111} + {100} also becomes active at 170 °C with a lower CO conversion and achieves a CO conversion of 39.8% at 220 °C. However, cubic Cu_2O only becomes active at 190 °C and achieves a CO conversion of 31.9% at 220 °C. In fact, it should be pointed out that the starting conversion temperature of cubic Cu_2O {100} is 20 °C higher than the two other samples. The starting CO conversion at 170 °C of truncated concave octahedral Cu_2O {332} + {100} is higher than that of truncated octahedral Cu_2O {111} + {100}. This phenomenon suggests that among the three types of samples, truncated concave octahedral Cu_2O {332} + {100} actually possesses the lowest activation barrier and cubic Cu_2O {100} possesses the highest activation barrier for CO oxidation. In order to illustrate the activation energies of the three types of Cu_2O, the Arrhenius plot of the oxidation of CO catalyzed by three types of Cu_2O is shown in Fig. 4b. From Fig. 4b, the calculated apparent activation energy of truncated concave octahedral Cu_2O {332} + {100} was indeed the lowest (111.7 ± 4.0 kJ mol^{-1}), whereas the calculated apparent activation energy of cubic Cu_2O {100} was the highest (203.2 ± 4.6 kJ mol^{-1}). In order to eliminate size effects, the specific catalytic CO oxidation rates over different microparticles were calibrated with surface areas

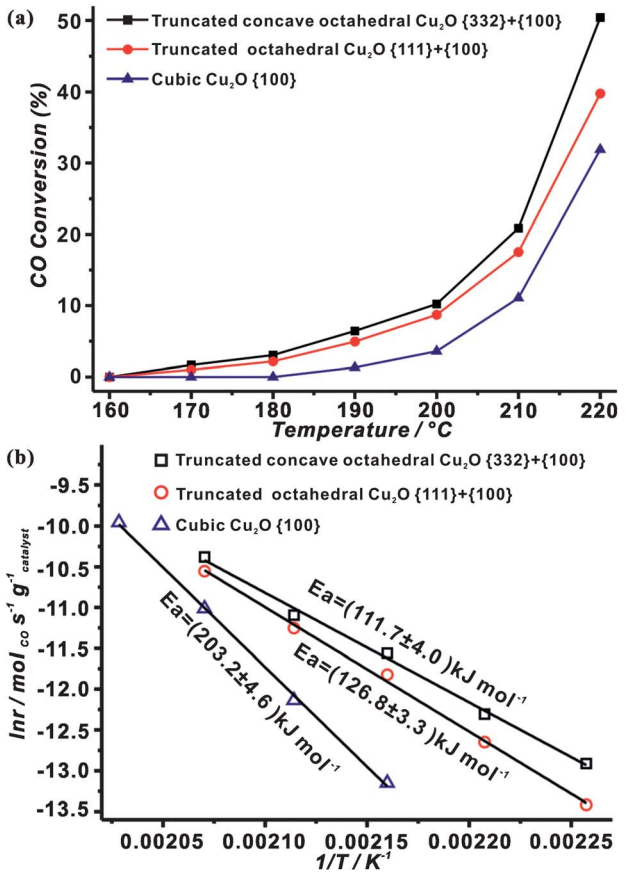

Fig. 4 (a) CO conversion of Cu_2O microparticles of different shapes as a function of temperature; (b) the Arrhenius plots of CO oxidation catalyzed by Cu_2O microparticles of different shapes.

using their average particle sizes (Fig. S10†). It was found that the specific catalytic CO oxidation rate of truncated concave octahedral Cu_2O {332} + {100} is still the highest and the specific catalytic CO oxidation rate of cubic Cu_2O {100} is the lowest from 190 °C to 220 °C. Therefore, from the experimental results above, it can be concluded that the order of CO catalytic activities of the crystal facets is {332} > {111} > {100}.

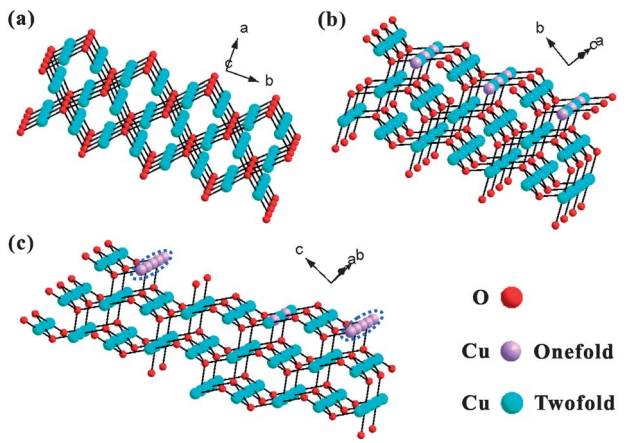

Fig. 5 Schematic models of (a) the (100) surface, (b) the (111) surface and (c) the (332) surface.

To study the catalytic activities of crystal facets, it is important to know whether the surface of catalysts was oxidized to CuO during the reaction, because Cu_2O might be oxidized to CuO at high temperature.[24,33] Therefore, the compositions and the morphologies of the catalysts were analyzed after CO oxidation. It was found that the bulk phases of three types of microcrystals still remain as the cubic phase of bulk Cu_2O after CO oxidation (Fig. S11†). And the morphologies of the three types of Cu_2O microcrystals did not change after CO oxidation (Fig. S12†). From XPS results, the Cu_2O microcrystals are stable during the catalytic measurement (Fig. S13†). Before CO oxidation, the peaks located at 932.7 eV and 952.6 eV can be respectively assigned to the binding energies of $Cu2p_{3/2}$ and $Cu2p_{1/2}$, which are characteristic values for Cu^I.[24,44,45] No peak showed the existence of Cu^{II}, which demonstrated that the surfaces of the three types of samples were not oxidized at ambient temperature. After CO oxidation, it was found that the binding energies of Cu are still located at 932.7 eV and 952.6 eV, which demonstrated that the Cu^I was not oxidized to Cu^{II} in the process of CO oxidation. Therefore, it can be determined that the surfaces of the three types of catalysts were not oxidized before and after catalytic measurement. The results of the catalytic reaction in Fig. 4 indeed show the different catalytic activities of different surfaces of Cu_2O microcrystals.

It is known that the CO oxidation on a solid catalyst involves an adsorption–oxidation–desorption process, which correlates closely with the surface structure. In principle, the catalytic activity for CO oxidation of Cu_2O depends on oxygen vacancies on the surface.[35] More oxygen vacancies can adsorb more ionized oxygen species and can react with the reducing gas more easily. Fig. 5 shows schematic models of Cu_2O (100), (111), and (332) surfaces. Cu atoms in the bulk Cu_2O are twofold-coordinated by O atoms, whereas copper atoms at the surface are usually coordinatively unsaturated. As shown in Fig. 5a, the Cu atoms on the (100) surface are coordinatively saturated. The (111) and (332) surfaces contain rows of twofold-coordinated Cu atoms (blue) and singly-coordinated Cu atoms (purple) with one dangling bond perpendicular to the surface (Fig. 5b and c). Thus, there are more dangling bonds on the (111) and (332) surfaces than on the (100) surface, which suggests that for adsorption of ionized oxygen species, the (111) and (332) facets of Cu_2O are more active. At the same time, Cu_2O (332) surface can be described as a combination of (111) terraces and (110) monoatomic steps. At the step edge, more dense singly-coordinated Cu atoms (purple) can be found as marked by the dotted circles in Fig. 5c, which further improve the activity of Cu_2O for adsorption of ionized oxygen species. Therefore, based on the surface structures, it can be concluded that for CO oxidation, the Cu_2O (332) surface is the most active and the Cu_2O (100) surface is the least active, which is consistent with the experiment results in Fig. 4.

Conclusions

In conclusion, we developed a facile wet chemical method to synthesize truncated concave octahedral Cu_2O microcrystals mainly enclosed by {*hhl*} high-index facets using an aqueous solution of $Cu(CH_3COO)_2$, SDS surfactant, NaOH, and D-(+)-glucose reductant. In this system, SDS was found to be

crucial for the formation of the concave Cu_2O microcrystals, and the crystal growth rate also affected the morphology of Cu_2O microcrystals. In the catalytic oxidation of CO, truncated concave octahedral Cu_2O enclosed mainly by {332} high-index facets exhibited enhanced catalytic activity in comparison with that of low index {111} and {100} facets, which could be due to the presence of high density steps on {332} high-index facets. The order of CO catalytic activities of the crystal facets was found to follow the sequence: {332} > {111} > {100}. These results above indicate that we can make use of surface-engineering strategies to improve the catalytic activity of materials due to the different activities of different crystal facets.

Acknowledgements

This work was supported by the National Basic Research Program of China (Grant no. 2011CBA00508), the National Natural Science Foundation of China (Grant nos. 21131005, 21021061, 21073145, and 21171141), and the Key Scientific Project of Fujian Province of China (Grant no. 2009HZ0002-1).

Notes and references

1 Z. Y. Zhou, N. Tian, J. T. Li, I. Broadwell and S. G. Sun, *Chem. Soc. Rev.*, 2011, **40**, 4176.
2 Z. Y. Jiang, Q. Kuang, Z. X. Xie and L. S. Zheng, *Adv. Funct. Mater.*, 2010, **20**, 3634.
3 H. Zhang, M. S. Jin and Y. N. Xia, *Angew. Chem., Int. Ed.*, 2012, **51**, 7656.
4 N. Tian, Z. Y. Zhou, S. G. Sun, Y. Ding and Z. L. Wang, *Science*, 2007, **316**, 732.
5 Y. Y. Ma, Q. Kuang, Z. Y. Jiang, Z. X. Xie, R. B. Huang and L. S. Zheng, *Angew. Chem., Int. Ed.*, 2008, **47**, 8901.
6 X. Q. Huang, Z. P. Zhao, J. M. Fan, Y. M. Tan and N. F. Zheng, *J. Am. Chem. Soc.*, 2011, **133**, 4718.
7 M. S. Jin, H. Zhang, Z. X. Xie and Y. N. Xia, *Angew. Chem., Int. Ed.*, 2011, **50**, 7850.
8 J. W. Zhang, L. Zhang, S. F. Xie, Q. Kuang, X. G. Han, Z. X. Xie and L. S. Zheng, *Chem.–Eur. J.*, 2011, **17**, 9915.
9 L. Zhang, J. W. Zhang, Q. Kuang, S. Xie, Z. Jiang, Z. Xie and L. Zheng, *J. Am. Chem. Soc.*, 2011, **133**, 17114.
10 T. Ming, W. Feng, Q. Tang, F. Wang, L. D. Sun, J. F. Wang and C. H. Yan, *J. Am. Chem. Soc.*, 2009, **131**, 16350.
11 F. Wang, C. H. Li, L. D. Sun, H. S. Wu, T. Ming, J. F. Wang, J. C. Yu and C. H. Yan, *J. Am. Chem. Soc.*, 2011, **133**, 1106.
12 Q. N. Jiang, Z. Y. Jiang, L. Zhang, H. X. Lin, N. Yang, H. Li, D. Y. Liu, Z. X. Xie and Z. Q. Tian, *Nano Res.*, 2011, **4**, 612.
13 L. Zhang, D. Q. Chen, Z. Y. Jiang, J. W. Zhang, S. F. Xie, Q. Kuang, Z. X. Xie and L. S. Zheng, *Nano Res.*, 2012, **5**, 181.
14 J. W. Zhang, L. Zhang, Y. Y. Jia, G. X. Chen, X. Wang, Q. Kuang, Z. X. Xie and L. S. Zheng, *Nano Res.*, 2012, **5**, 618.
15 X. H. Xia, J. Zeng, B. McDearmon, Y. Q. Zheng, Q. G. Li and Y. N. Xia, *Angew. Chem., Int. Ed.*, 2011, **50**, 12542.
16 F. Wang, C. H. Li, L. D. Sun, H. S. Wu, T. A. Ming, J. F. Wang, J. C. Yu and C. H. Yan, *J. Am. Chem. Soc.*, 2011, **133**, 1106.
17 H. Zhang, W. Y. Li, M. S. Jin, J. Zeng, T. K. Yu, D. R. Yang and Y. N. Xia, *Nano Lett.*, 2011, **11**, 898.
18 X. Q. Huang, Z. P. Zhao, J. M. Fan, Y. M. Tan and N. F. Zheng, *J. Am. Chem. Soc.*, 2011, **133**, 4718.
19 M. R. Gao, Z. Y. Lin, J. Jiang, H. B. Yao, Y. M. Lu, Q. Gao, W. T. Yao and S. H. Yu, *Chem.–Eur. J.*, 2011, **17**, 5068.
20 Z. Y. Wang, D. Y. Luan, C. M. Li, F. B. Su, S. Madhavi, F. Y. C. Boey and X. W. Lou, *J. Am. Chem. Soc.*, 2010, **132**, 16271.
21 X. W. Xie, Y. Li, Z. Q. Liu, Q. Haruta and W. J. Shen, *Nature*, 2009, **458**, 746.
22 H. G. Yang, C. H. Sun, S. Z. Qiao, J. Zou, G. Liu, S. C. Smith, H. M. Cheng and G. Q. Lu, *Nature*, 2008, **453**, 638.
23 X. G. Han, Q. Kuang, M. S. Jin, Z. X. Xie and L. S. Zheng, *J. Am. Chem. Soc.*, 2009, **131**, 3152.
24 M. Leng, M. Z. Zhang, Y. B. Wang, Z. Q. Yu, C. Yang, X. G. Zhang, H. J. Zhang and C. Wang, *J. Am. Chem. Soc.*, 2010, **132**, 17084.
25 X. G. Han, M. S. Jin, S. F. Xie, Q. Kuang, Z. Y. Jiang, Y. Q. Jiang, Z. X. Xie and L. S. Zheng, *Angew. Chem., Int. Ed.*, 2009, **48**, 9180.
26 X. Wang, X. G. Han, S. F. Xie, Q. Kuang, Y. Q. Jiang, S. B. Zhang, X. L. Mu, G. X. Chen, Z. X. Xie and L. S. Zheng, *Chem.–Eur. J.*, 2012, **18**, 2283.
27 X. M. Zhou, J. Y. Lan, G. Liu, K. Deng, Y. L. Yang, G. J. Nie, J. G. Yu and L. J. Zhi, *Angew. Chem., Int. Ed.*, 2012, **51**, 178.
28 W. C. Huang, L. M. Lyu, Y. C. Yang and M. H. Huang, *J. Am. Chem. Soc.*, 2012, **134**, 1261.
29 M. Hara, T. Kondo, M. Komoda, S. Ikeda, K. Shinohara, A. Tanaka, J. N. Kondo and K. Domen, *Chem. Commun.*, 1998, 357.
30 Y. Yamada, K. Yano and S. Fukuzumi, *Energy Environ. Sci.*, 2012, **5**, 5356.
31 A. O. Musa, T. Akomolafe and M. J. Carter, *Sol. Energy Mater. Sol. Cells*, 1998, **51**, 305.
32 P. Poizot, S. Laruelle, S. Grugeon, L. Dupont and J. M. Tarascon, *Nature*, 2000, **407**, 496.
33 H. Z. Bao, W. H. Zhang, Q. Hua, Z. Q. Jiang, J. L. Yang and W. X. Huang, *Angew. Chem., Int. Ed.*, 2011, **50**, 12294.
34 L. L. Li, C. Y. Nan, Q. Peng and Y. Li, *Chem.–Eur. J.*, 2012, **18**, 10491.
35 T. J. Huang and D. H. Tsai, *Catal. Lett.*, 2003, **87**, 173.
36 J. Y. Ho and M. H. Huang, *J. Phys. Chem. C*, 2009, **113**, 14159.
37 H. Pang, F. Gao and Q. Y. Lu, *CrystEngComm*, 2010, **12**, 406.
38 Y. M. Sui, W. Y. Fu, Y. Zeng, H. B. Yang, Y. Y. Zhang, H. Chen, Y. X. Li, M. H. Li and G. T. Zou, *Angew. Chem., Int. Ed.*, 2010, **49**, 4282.
39 H. Yang and Z. H. Liu, *Cryst. Growth Des.*, 2010, **10**, 2064.
40 D. F. Zhang, H. Zhang, L. Guo, K. Zheng, X. D. Han and Z. Zhang, *J. Mater. Chem.*, 2009, **19**, 5220.
41 K. X. Yao, X. M. Yin, T. H. Wang and H. C. Zeng, *J. Am. Chem. Soc.*, 2010, **132**, 6131.
42 M. A. Vanhove and G. A. Somorjai, *Surf. Sci.*, 1980, **92**, 489.
43 Y. Y. Ma, Z. Y. Jiang, Q. Qin, S. H. Zhang, Z. X. Xie, R. B. Huang and L. S. Zheng, *J. Phys. Chem. C*, 2008, **112**, 13405.
44 A. Radi, D. Pradhan, Y. Sohn and K. T. Leung, *ACS Nano*, 2010, **4**, 1553.
45 Y. C. Mao, J. T. He, X. F. Sun, W. Li, X. H. Lu, J. Y. Gan, Z. Q. Liu, L. Gong, J. Chen, P. Liu and Y. X. Tong, *Electrochim. Acta*, 2012, **62**, 1.